Osteogenesis of Mesenchymal Stem Cells by Nanoscale Mechanotransduction

Habib Nikukar,[†,§] Stuart Reid,[‡,*] P. Monica Tsimbouri,[†] Mathis O. Riehle,[†] Adam S. G. Curtis,[†] and Matthew J. Dalby[†,*]

[†]Centre for Cell Engineering, Institute for Molecular, Cell and Systems Biology, College of Medical, Veterinary and Life Sciences, University of Glasgow, Glasgow G12 8QQ, United Kingdom, [‡]SUPA, Thin Film Centre, University of the West of Scotland, Paisley PA1 2BE, United Kingdom, and [§]Shahid Sadoughi University of Medical Sciences, Yazd, I. R. Iran

ABSTRACT It is likely that mesenchymal stem cells will find use in many autologous regenerative therapies. However, our ability to control cell stem growth and differentiation is presently limited, and this is a major hurdle to the clinical use of these multipotent cells especially when considering the desire not to use soluble factors or complex media formulations in culture. Also, the large number of cells required to be clinically useful is currently a hurdle to using materials-based (stiffness, chemistry, nanotopography, *etc.*) culture substrates. Here we give a first demonstration of using nanoscale sinusoidal mechanotransductive protocols (10−14 nm displacements at 1 kHz frequency), "nanokicking", to promote osteoblastogenesis in human mesenchymal stem cell cultures. On the basis of application of the reverse piezo effect, we use interferometry to develop the optimal stem cell stimulation conditions, allowing delivery of nanoscale cues across the entire surface of the Petri dishes used. A combination of immunofluorescence, PCR, and microarray has then been used to demonstrate osteoblastogenesis, and the arrays implicate RhoA as central to osteoblastic differentiation in agreement with materials-based strategies. We validate this with pharmacological inhibition of RhoA kinase. It is easy to envisage such stimulation protocols being up-scaled to form large-scale osteoblast bioreactors as standard cell culture plates and incubators are used in the protocol.

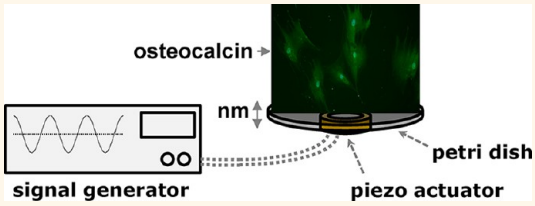

KEYWORDS: nanoscale · mechanotransduction · osteogenesis · mesenchymal stem cells

It has been well-established that many cell types can respond to a variety of nanoscale cues, most notably with nanotopographies and nanoparticles.[1−8] Cell responses include significant changes in adhesion, migration, morphology, and gene expression. More recently, research has demonstrated that nanotopography alone can stimulate targeted osteogenesis[9,10] and self-renewal[11] in mesenchymal stem cells (MSCs).

MSCs are multipotent cells that can be isolated from the bone marrow[12] (as used in this study) or other tissues such as dental tissue,[13] adipose tissue,[14] or umbilical cord.[15] They have the potential to form cells of the bone, cartilage, adipose, and reticular tissues and are sometimes also implicated in smooth muscle[16] and even neural cell lineages.[17]

Use of nanotopographies has shown that the shift from stem cell to differentiated osteoblast is regulated through changes in adhesion and intracellular tension.[18] This result is consistent with the fact that osteoblasts, which possess larger cell morphology than, for example, adipocytes, fibroblasts, and MSCs, require large adhesions to support the tensile cytoskeletal scaffolding.[18,19] Such effects have also been observed in MSCs cultured on hydrogels[20] or forced to confine to morphologies using microcontact printing of fibronectin.[21−23] By modifying the gel rigidity, soft gels were observed to promote expression of neural markers as cells lost the ability to generate intracellular tension through deformation of the compliant gel substrate. Conversely on the harder gels, with similar stiffness to precalcified bone at 40 kPa, the cells were able to retain intercellular tension as a result of large adhesion complexes and thus differentiate to osteoblasts.[20]

An interesting study on MSC confinement used an array of small (1000 μm^2) fibronectin microcontact printed squares

* Address correspondence to matthew.dalby@glasgow.ac.uk, stuart.reid@uws.ac.uk.

Received for review January 14, 2013 and accepted February 27, 2013.

Published online February 27, 2013
10.1021/nn400202j

© 2013 American Chemical Society

(among a low adhesion, PEG background), preventing spreading of cells, therefore, inhibiting intracellular tension and ultimately leading to the formation of adipose (fat) tissue. However, when spreading was actively promoted on larger, 10 000 μm^2, fibronectin squares, cells formed large adhesion complexes with a well-organized cytoskeleton, resulting in differentiation to osteoblasts.[21] An elegant update on this study used printed fibronectin star and flower shapes to demonstrate that even when MSCs are dimensionally confined, features that promote adhesion (such as the sharp corners of the star shapes) promote intracellular tension and thus osteogenesis. Conversely, features that reduce adhesion (such as the softer contours of the flower pattern) significantly reduce intracellular tension and therefore prevent osteoblastic differentiation.[23]

The commonality of all of the above studies is investigation of the RhoA kinase pathway (ROCK) as a key modulator of osteogenesis. This result is explicable since RhoA is a small G-protein involved in the activation of actin/myosin contraction. Cells require this cytoskeletal contraction mechanism in order to spread and to migrate. The intracellular actin microfilaments are located onto focal adhesions on the cell membrane, against which (with myosin) they pull. As discussed, osteoblasts are a large progeny of MSCs and are typically very well spread, thus a highly contracted cytoskeleton is required to support this phenotype, and this generates high intracellular tension. In addition, focal adhesions and the cytoskeleton network are in a force−balance relationship such that a highly contractile cytoskeleton requires large focal adhesions and large focal adhesions require force to gather integrins and hence to grow.[24−28] It is notable that osteoblasts have a high proportion of supermature, or fibrilar, adhesions (adhesions >5 μm in length).[29,30]

It appears that, as cells form adhesions, the plasma membrane creates nanoscale vibrations, which help determine how the cell interacts with the surface.[24] It is the aim of this study to see if we can feedback these vibrations to the cells to target MSC differentiation. That is, if we settle the cells on surfaces that vibrate on the nanoscale, does this affect MSC adhesion and ultimately phenotype?

At the macro- and microscale, a wide variety of cells, including MSCs, have been shown to respond to stress and strain.[31−34] In fact, mechanical stimulation is a common strategy in tissue engineering of cartilage and ligament, for example.[35−38] This is because mechanical alterations in cell morphology lead to changes in cell signaling and gene transcription. Indeed, not only mechanical load patterns but also electrical and electromagnetic stimulation patterns have been shown to be efficacious in neural and bone regeneration.[39−41]

Focusing on focal adhesions as a mechanoreceptor, but being mindful there are others, alterations in adhesion formation lead to changes in cell tension and G-protein signaling. However, this may also impact focal adhesion kinase (FAK) and extracellular signal-related kinase (ERK) signaling cascades,[32,42,43] which are intimately linked to activation of transcription factors, such as runt-related transcription factor 2 (RUNX2), responsible for transcription and thus expression of bone-related genes such as osteocalcin.[44−46]

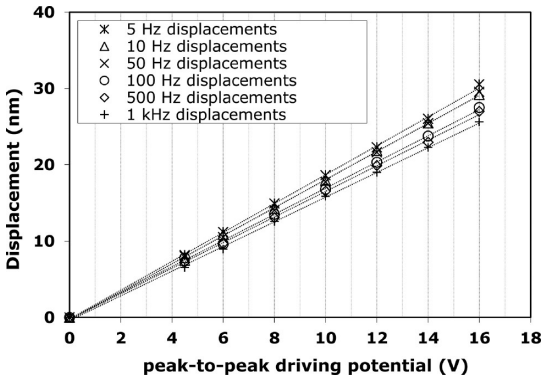

Figure 1. Displacement (nm) as a function of electrical potential (V) at different frequencies measured at the surface of the piezo actuator by interferometry.

In this report, the reverse piezo effect is used to stimulate MSCs. A potential is applied to a piezo ceramic actuator causing expansion. The actuator can be driven so that both the frequency and amplitude of the displacement can be accurately and reproducibly controlled to deliver nanoscale "kicks" to MSCs.

RESULTS

Experimental Setup. Through use of laser interferometry, it was demonstrated that reproducible nanoscale excursions could be produced at different driving frequencies, up to 1 kHz. These were in the range of 5−30 nm depending on applied potential (Figure 1). An aluminum block, of approximate dimensions 320 × 100 × 50 mm, was used to provide a stable, rigid base in order to direct the majority of the displacement upward to the Petri dish. In addition, an aluminum disk, of 50 mm diameter and 3 mm thickness, was rigidly glued between the piezo ceramic and the polystyrene tissue culture Petri dish (a 60 mm diameter dish, but the usable bottom surface is 52 mm in diameter) to minimize the deviation in the displacements that were observed across the surface of the dish (Figures 2 and 3). Displacements were typically observed to reduce as the driving frequency increased. For the stimulation frequencies that will be used for promoting osteogenesis here, the average decrease in the displacement was observed to be 5.3% and therefore assumed to be negligible. Further schematics of the experimental setup are provided in the Supporting Information Figures 1 and 2.

Selection of Frequency. By continuous sine wave drive, 10 V was chosen as the peak-to-peak driving potential

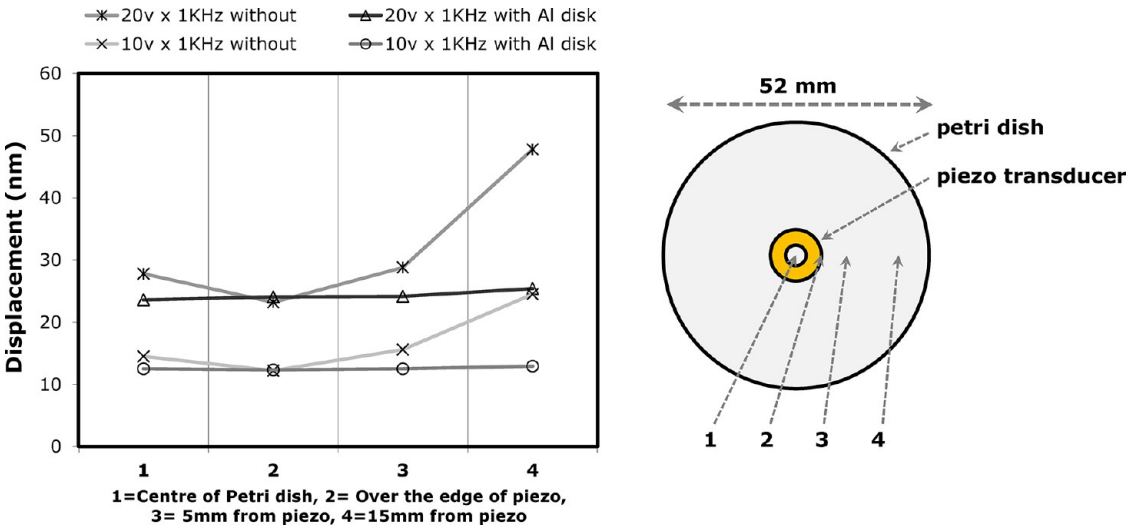

Figure 2. Comparison of displacement measurements with (solid) and without (dashed) the addition of an aluminum disk that showed a significantly reduced deviation in the observed displacements after applying the disk to the 52 mm diameter Petri dishes. When the aluminum disks were not used, large central and peripheral displacements were noted due to a flapping effect. The experiment was performed at 10 or 20 V driving potentials and at 1 kHz frequency. Numbers 1 to 4 represent distances from the center (1 = center, 2 = above piezo, 3 = 5 mm from piezo edge, 4 = 15 mm from piezo edge).

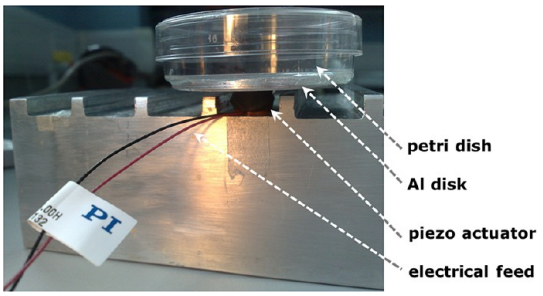

Figure 3. Image of the typical setup, with 52 mm diameter Petri dish and attached piezo actuator glued between the large aluminum block (below) to ensure upward movement on expansion of the piezo and the aluminum disk to provide low dispersion in the center to edge displacements.

for a wide range of sinusoidal frequencies when stimulating the MSCs. These were 25, 50, 100, 500, and 1000 Hz frequencies giving displacements of 14.25, 12.5, 11.17, 13.91, and 12.57 nm, respectively. Gene transcript, RT-PCR analysis for the osteogenic transcription factor RUNX2 revealed that it was only up-regulated compared to static control on the 1 kHz frequencies (supplementary Figure 3). Thus, 1 kHz was chosen as our optimal frequency, and the closest lower frequency, 500 Hz, was also used as another control below osteogenic induction. In order to use the higher, 1 kHz, frequency moving forward, effects of heating (supplementary Figure 4), shear, and fluid motion were ruled out (data not shown here); that is, there were no differences to static control.

Osteogenic Analysis. Transcriptional analysis by quantitative real-time (qRT-) PCR for bone morphogenic protein 2 (BMP2) after 24 h culture, densitometry quantified gel RT-PCR for RUNX2, and gene microarray after 1 week of culture showed that, while 500 Hz caused a significant shift of total genomic expression, BMP2 and RUNX2 expression was not altered (Figure 4A–C). This indicates that, while 500 Hz causes a shift in gene expression profile, it is not large enough to trigger osteogenesis from the MSCs. However, at 1 kHz, the genomic shift was again noted (larger shift than with 500 Hz stimulation), although this time, concomitant significant changes in BMP2 and RUNX2 expression were observed. This speculatively suggests that a threshold of a change in genomic regulation has occurred to permit osteogenesis. Given longer in culture (14 days of stimulation) and using antibodies against the RUNX2-regulated bone-specific marker protein osteocalcin,[47] the result was verified as it was again shown that 500 Hz did not induce significant change from control but that 1 kHz stimulation caused a large increase in protein expression (Figure 4D,E).

Uploading array data for 1 kHz stimulation to Ingenuity pathway analysis revealed significant changes in regulation in pathways involved in tissue development (most significantly, for this study, skeletal and muscular system development and function; skeletal and muscular system share common stem cell origin). Also noted were cell growth and small molecule biochemistry (likely linked to energy demand as lipid and carbohydrate metabolism) (Figure 5).

ROCK Inhibition. Immunofluorescence of vinculin (involved in focal adhesions) and actin cytoskeleton revealed that MSCs stimulated at 1 kHz compared to control cells were more spread (quantified in supplementary Figure 5), with larger focal adhesions and well-organized cytoskeletal contraction fibers (Figure 6). This is highly suggestive of increased intracellular tension with nanoscale stimulation.

Using Ingenuity to observe canonical, biochemical signaling pathways rather than functional pathways,

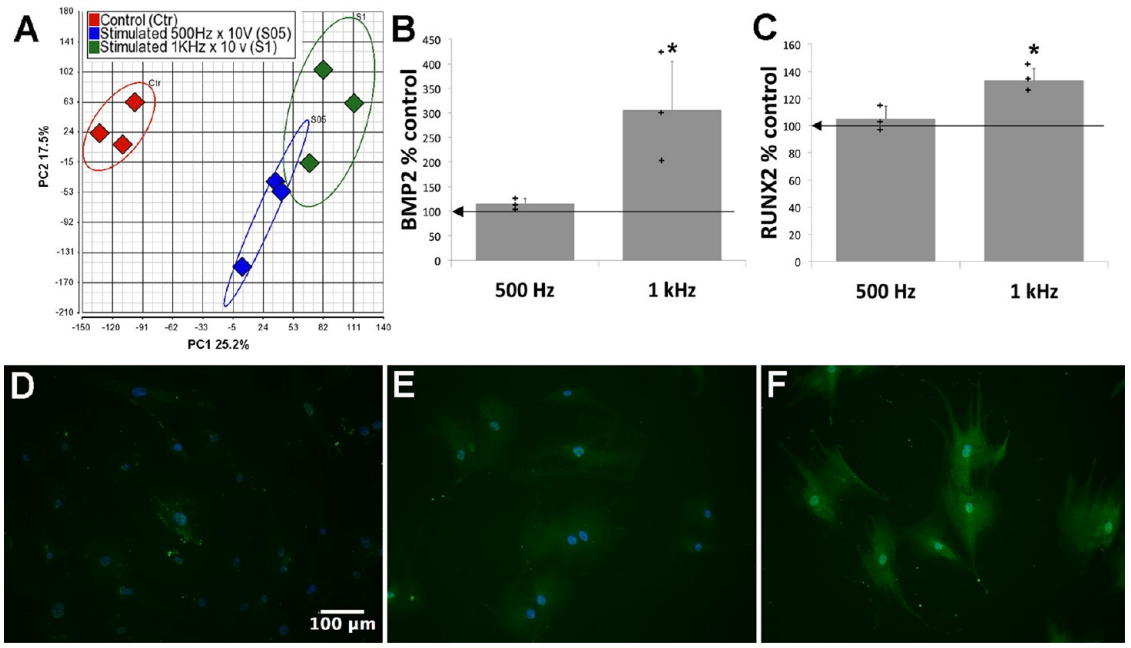

Figure 4. Transcriptional analysis: (A) Microarray principle component analysis showing large shifts of gene regulation from MSCs on control after 1 week of culture. The changes were greatest (from control) for MSCs stimulated at 1 kHz. The graph shows that the main component (PC1) accounts for 25.7% of differences and the secondary component (PC2) accounts for 17.5% of differences. (B) qRT-PCR of BMP2 expression showing increased expression in response to 1 kHz stimulation but not 500 Hz after 24 h of culture. (C) Densitometry from RT-PCR gels showing no change in RUNX2 expression between control and 500 Hz stimulation, but up-regulation after 1 kHz stimulation for 1 week. Looking at protein expression of the osteoblast marker, osteocalcin, after 14 days showed increased expression in response to 1 kHz stimulation (F) compared to control (D) of 500 Hz (E) (green = osteocalcin, blue = nucleus). For PCR, $n = 3$ (one experiment with three materials replicates for qPCR, and another experiment with three materials replicates for RT-PCR); results are mean ± standard deviation, $*p < 0.05$ by ANOVA, + = individual data points used to calculate mean and standard deviation; arrow shows control mean.

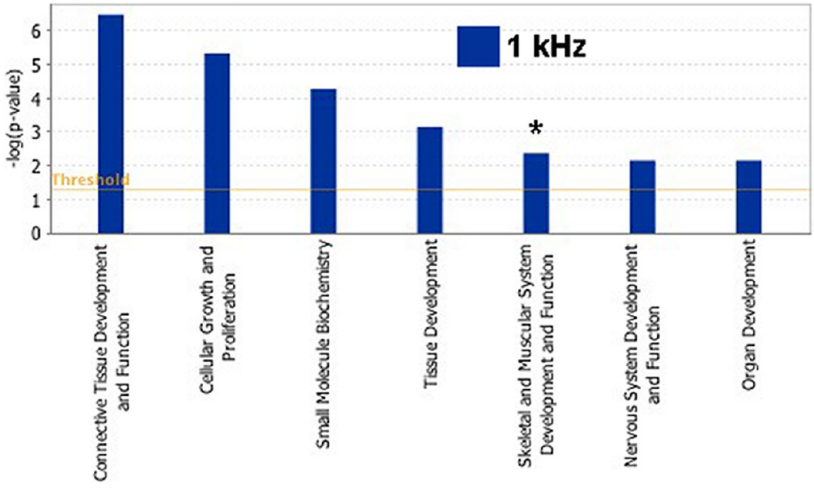

Figure 5. Functional pathway analysis. Among the highlighted pathways differentially regulated after 1 week with 1 kHz stimulation are cell growth, organ, and tissue development and skeletal and muscular system development and function. $N = 3$, threshold = $p < 0.05$ compared to unstimulated control. * Denotes skeletal system development.

it was seen that ROCK signaling was highlighted as significantly changed with stimulation (Figure 7). Furthermore, network analysis implicated roles for adhesion, FAK, ERK, actin, and sonic hedgehog signaling as well as RhoA signaling (see canonical pathway (CP) tags linked into the network) (Figure 8). It is noteworthy that this network illustrates the input of these biochemical pathways into genes controlling cell growth, proliferation, and division. In the classical Stein and Lian[48] osteogenic timelines, day 7 is when maximal proliferation is seen in cells undergoing osteogenesis compared to control cultures; the array was performed at day 7, and it is thus sensible that these regulatory genes were seen to be up-regulated.

That RhoA signaling is implicated (Figures 7 and 8) is clearly interesting as it has been highlighted as being

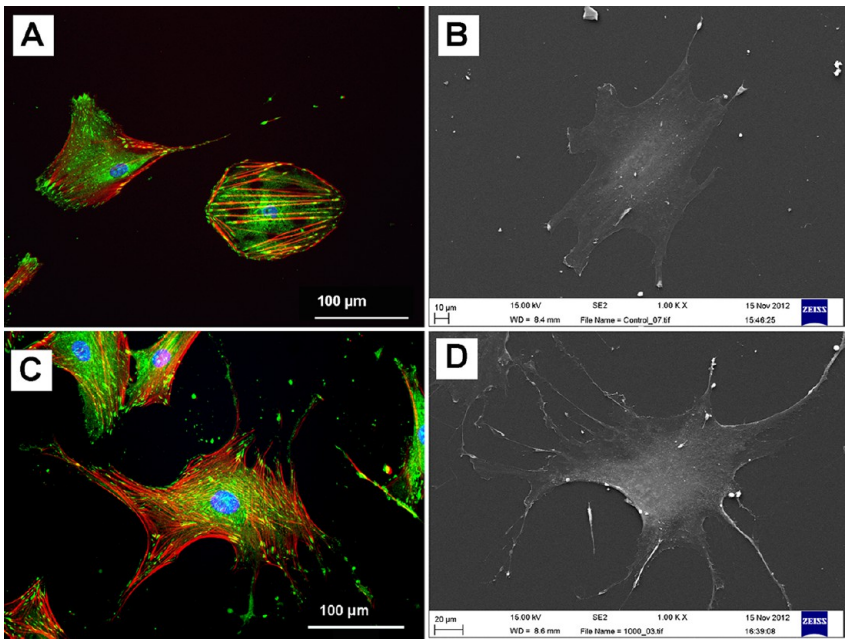

Figure 6. Morphology, focal adhesion, and actin cytoskeleton staining. (A) On unstimulated control, cells were smaller with actin stress fibers terminating at focal adhesion sites. (B) MSCs were seen to have a standard morphology. (C) With 1 kHz stimulation, cells were larger, more polygonal, and tended to have both larger and more adhesions with well-organized actin stress fibers and long cellular processes. (D) Electron micrograph of a typical MSC stimulated at 1 kHz with long cellular projections. For fluorescent images red = actin, green = vinculin, and blue = nucleus.

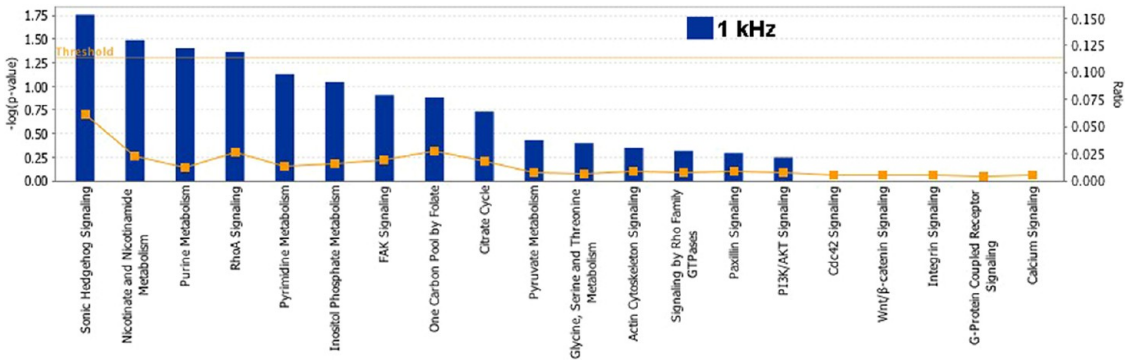

Figure 7. Canonical pathway analysis. A significantly altered canonical pathway is RhoA signaling (asterisk). Also significantly altered from unstimulated control are sonic hedgehog signaling, purine and nicotinamide metabolism. $N = 3$, threshold = $p < 0.05$.

central to osteogenesis in seminal studies.[21,23] Using Y27632 to inhibit ROCK activity, it was seen that MSCs' ability to express osteocalcin was reduced with inhibition, confirming its role in our nanostimulation system (supplementary Figure 6).

DISCUSSION

For the first time, it is shown that MSCs are responsive to vertical nanoscale mechanical excursions. Furthermore, it was demonstrated that this osteoblastogenic response was ROCK-dependent, in agreement with previous materials-based strategies for osteoinduction.[11,20−23] That ROCK inhibition blocked osteoblastogenesis demonstrates that the stimulation is a real effect. Furthermore, that BMP2 is activated by 24 h and RUNX2 by 7 days is logical, as RUNX2 activity is mediated by BMP2 signaling,[49,50] this would be followed by increased osteocalcin expression by day 14 according to the Stein and Lian osteoblastogenesis timelines.[38] Ingenuity canonical analysis also highlights purine and nicotinamide metabolism (involved in energy demand) and sonic hedgehog signaling (involved is stem cell differentiation)[51] as well as adhesion, FAK, ERK, and actin-mediated biochemical signaling (all known to be implicated in RUNX2 activation)[19,29,45,46,52] being central to nanomechanotransduction.[53,54]

Use of an open hypothesis for input frequency led to use of 1 kHz. This appears high for the time scale of many cell actions. Pierres *et al.*[55] provide an interesting perspective article on cell membrane undulations based on their original data[31] and the literature. They first note that many familiar, conventional membrane

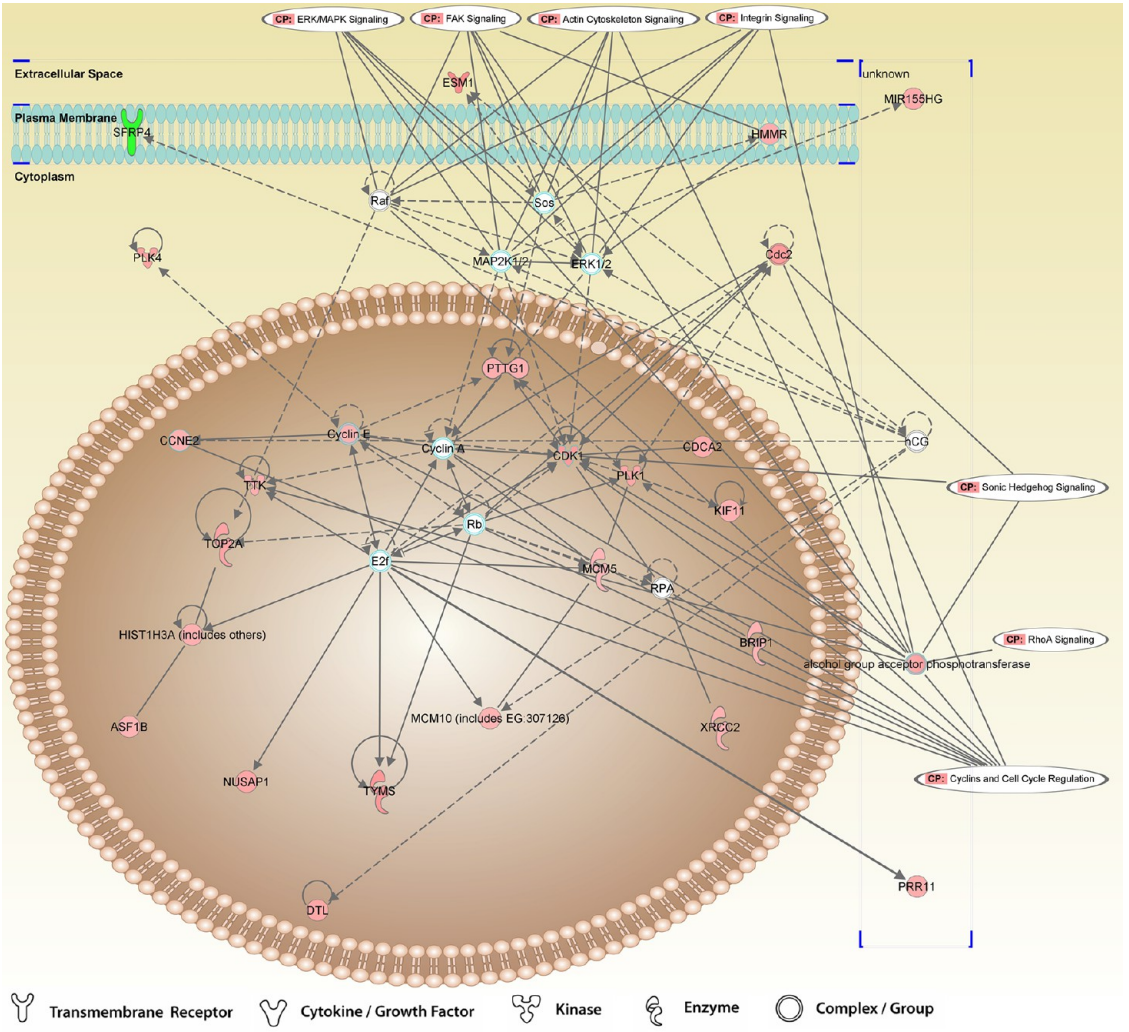

Figure 8. Network analysis showing involvement of focal adhesion, FAK, ERK, actin, sonic hedgehog, and RhoA signaling in response to 1 kHz nanomechanostimulation. *N* = 3. Note that CP = canonical pathway and the lines into the network indicate where these biochemical pathways are involved in the network. The network illustrates gene interactions involved in growth, proliferation, and division (solid line = direct interaction, dashed lines = indirect interaction). Genes are compartmentalized as external, membrane-bound, cytoplasmic, and nuclear (green = down-regulation, red = up-regulation, white = not tested (below quality threshold or not on the array)).

deformations occur at the tens of seconds time scale, such as filopodial probing (filopodia are actin-driven projections used to "probe" the extracellular environment for adhesion points).

However, they next note that many cell membrane interactions occur much faster than this. For example, neutrophils completely ingest pathogens within seconds[56] and endothelial arrest of flowing leukocytes involves subsecond integrin activation.[57] The authors point out that subsecond membrane undulations may be key to these phenomena. Interestingly, erythrocyte membranes display high-frequency undulations as high as 1 kHz in the tens of nanometers range called flickering[58,59]—this is very similar scale to the stimulation we supply the cells with in this report. However, it is noted that such movements have been noted as being slower in nucleated cells such as lymphocytes and monocytes from blood displaying 20−30 nm undulations at up to 30 Hz and fibroblasts (descendants of MSCs) displaying 1−4 nm displacements at up to 0.5 Hz.[60−62]

Over a number of years, there has been discussion of piezoelectic effect in bone. This is because, while collagen is piezoelectric when dry, for effect to be seen in hydrated bone, kilohertz range stimulus is required, that is, beyond that considered physiological.[63] Furthermore, it is known that electricity can be used to guide cells (galvanotaxis)[64,65] and stimulate bone repair.[66] It has been postulated that bones' piezoelectrical properties facilitate osteoblast activity as they are attracted by the electrical dipoles produced by piezoelectricity or deformation of the bone,[67] and modeling has been used to show that piezo effects could be important in bone homeostasis with mechanical loads leading to polarization of bone, suggesting that negative charges accumulate at sites of bone removal and

positive charges at sites of bone formation.[68] However, we note that while it is tempting to try and draw parallels between the values obtained for piezoelectic effect in bone, the benefit to bone of electrical stimulation, and the 1 kHz osteogenic stimulation we have used here, it is far too speculative, at this stage, to do so.

In addition to describing the details of the applied motion in terms of frequency and amplitude, it may also be of interest to consider the forces being applied to each cell. During the MSC stimulation presented here, a periodic force is imposed on each cell through the Petri dish substrate. Since the cells are adherent to the substrate surface prior to stimulation, this force is transmitted through each cell as it supports the column of aqueous solution directly above. Taking approximations for the cell shape (adhered surface area typically a few tens of micrometer $\times$ a few tens of micrometers) and height of solution (3→5 mm), the accelerative force on each cell can be calculated to be in the range of 1→10 pN. This can be calculated from Newton's second law, $F_{acc} = ma$, where the accelerative force, F_{acc}, driving the motion of the column of water with acceleration, a, and with mass, m, must be transmitted through the cell to the oscillating substrate surface. Note that these forces are of a similar order of magnitude to the forces exerted by fibroblast undulations, observed in the range of 20→80 pN.[61] Further investigations are required to evaluate the precise mechanisms responsible for how MSCs sense these applied mechanical forces.

CONCLUSION

We introduce a new nanoscale method of MSC stimulation for targeted osteoblastogenesis. This does not rely on novel materials, complex chemistry, or electronic clean room facilities. Rather, it is based on traditional cell culture plastics with simple addition of piezo ceramics. Up-scale to bioreactors that can prime autologous MSCs to form osteoblasts without recourse to soluble factors can be easily envisaged. Furthermore, we note that whole body vibration is becoming adopted in the clinic to help with musculoskeletal regeneration following, for example, spinal trauma, osteoporosis, and stress fracture repair.[69,70] It could thus be envisaged that *in vitro* experiments could be used to inform therapy with the noted caveat that the modeling from cell to whole body is nontrivial and much research aimed at practical/theoretical scaling between nanoscale cell culture and the human body is required. Such techniques could be complementary to existing external stimuli for musculoskeletal regeneration such as extracorporeal shock wave treatment.[71]

MATERIALS AND METHODS

Setup. The piezo actuators were driven by continuous sine wave using an Agilent 33210A function generator in combination with a DC offset circuit for maintaining positive-only voltages applied with the same polarity as the poling voltage used in the piezo manufacture. The piezo actuators used in all of the reported investigations were supplied by Physik Instrumente GmbH (Germany), model number 010-05H ring-type piezo stacks. This experimental setup, as shown in Figure 3 and supplementary Figures 1 and 2, was used for supplying vertical displacements to MSC cultures.

Calibration. The calibration of individual piezo devices and the displacement measurements across the surface of the Petri dishes were performed using a SIOS interferometer, model SP-S120 laser interferometric vibrometer. The response of the individual piezo devices was observed to be linear with driving voltage, with deviations typically less than a few percent. The response was also observed to be linear with respect to frequency, with the displacement being observed to decrease by typically 10−15% from 50 Hz to 1 kHz. The measured displacements across empty Petri dishes were observed to typically vary by 10−15%, around a 3-fold decrease in the variability as compared to Petri dishes that were not supported on their underside by a 3 mm thick aluminum disk.

Thermal Check. Since the piezo actuators have to do work against the Petri dish assembly, it can be assumed that heat is generated. If the power dissipated within the piezo ceramic material transfers through conduction to the aluminum disk, the polystyrene Petri dish, and ultimately to the culture solution, then there exists the possibility of thermal shock to the cells. To evaluate the possibility of thermal shock to the cell cultures, a thermal imaging was used to estimate the degree of heating during stimulation. As shown in supplementary Figure 4, the effect of heating can be assumed to be negligible in these investigations.

Viscous and Shear Forces. As previously detailed in the Calibration section, care was undertaken to ensure that the stimulation setup acted as a rigid body, transmitting equal displacements across the surface of the culture substrate. Therefore, displacements are expected to be closely confined to the vertical direction and thus minimize the possibility of fluid flow, which could promote large viscous forces on the cells. Shear forces are also expected to remain negligible.

Cell Culture. MSCs were purchased from Promocell (Germany) and used at passages 1−3. MSCs were maintained in basal media (aMEM (PAA)) supplemented with 10% FBS (PAA), 1% (v/v) 200 mM L-glutamine (Gibco), and antibiotics (6.74 U/mL penicillin-streptomycin, 0.2 μg/mL fungizone) (PAA) at 37 °C with 5% CO_2 in an incubator. Cells were seeded into the Petri dishes at 1 $\times$ 10^4 cells/mL, and medium was changed every 3 days. For inhibition studies, Y27632 (Sigma), a ROCK inhibitor, was used at 10 μM concentration throughout each experiment.

Immunofluorescence. MSCs were fixed in a 10% formaldehyde solution, permeabilized and blocked in 1% (w/v) BSA/PBS, and stained with anti-osteocalcin and anti-RUNX2 (1:50) (Santa Cruz Biotechnology) or anti-vinculin (1:200) (Clone hVin-1, Sigma) in 1% (w/v) BSA/PBS and incubated at 37 °C for 1 h, in conjunction with phalloidin-rhodamine (1:200) (Molecular Probes). Cells were washed 3 $\times$ 5 min in 1$\times$ PBS/0.5% Tween-20 and a biotinylated secondary anti-mouse antibody (Vector Laboratories) was added at 1:50 in 1% (w/v) BSA/PBS and incubated at 37 °C for 1 h. After being washed, the samples were incubated with FITC-conjugated streptavidin (1:50, Vector Laboratories) for 30 min at 4 °C, washed, and mounted using Vectashield mountant with DAPI nuclear stain (Vector Laboratories).

Scanning Electron Microscopy. MSCs were cultured and stimulated for 7 days prior to fixing. After 1 h incubation of samples at 4 °C in a mixture of 1.5% glutaraldehyde + 0.1 M sodium cacodylate (buffer fix), the dishes were rinsed by 0.1 M sodium cacodylate 3 $\times$ 5 min. Then 1% osmium tetroxide was added for 1 h in room temperature, followed by distilled water (DW) wash (3 $\times$ 10 min each). Uranyl acetate was then added for 1 h incubation in the dark, followed by a quick DW rinse and

TABLE 1. Primer Details for PCR

gene	forward primer	reverse primer
RUNX2	CAGACCAGCAGCACTCCATA	CAGCGTCAACACCATCATTC
BMP2	ATGGATTCGTGGTGGAAGTG	GTGGAGTTCAGATGATCAGC
GAPDH	GTCAGTGGTGGACCTGACCT	ACCTGGTGCTCAGTGTAGCC

ethanol dehydration series (30, 50, 70, 90, 100% followed by a dried absolute ethanol wash). After being washed two times for 5 min each by hexamethyl disilazane (HMDS), the samples were left overnight for gradual evaporation prior to coating. Using a Polaron SC515 SEM coating system, the samples were coated by gold palladium (about 18 nm coverage thickness) and then they were cut into circles (15 mm diameter) and stuck onto aluminum stubs. A Carl Zeiss Sigma variable-pressure analytical SEM with Oxford Microanalysis was used to image the samples.

RT-PCR (Agarose Gel Electrophoresis). MSCs were cultured and treated in the Petri dishes for 7 days with three replicas for each condition. Total RNA was extracted using a Qiagen RNeasy micro kit. Reverse transcription of extracted RNA to cDNA was performed using the Omniscript reverse transcription kit (Qiagen) according to the manufacturer's protocol. For efficient cDNA amplification, the GoTaq Hot Start Green Master Mix was used in combination with gene-specific primers (Table 1) and a thermal cycler program for 30 cycles (2 min 95 °C hold followed by cycles 30 s in 95, 55, and 72 °C each and 5 min in 72 °C as the final stage). Amplified cDNAs from three replicas in a control group and stimulated groups were run on a 1% agarose gel beside a 100 bp ladder, and the expression of RUNX2 was compared between groups of samples.

Quantitative Real-Time (qRT-) PCR. Total RNA was extracted from three replicas for every condition using a Qiagen RNeasy micro kit. Real-time qPCR was performed and analyzed as previously described to assess the expression of RUNX2 and BMP2 (Table 1). RNA samples were reverse transcribed using the Omniscript First Strand synthesis kit (Qiagen). qRT-PCR was carried out using the 7500 Real Time PCR system from Applied Biosystems. GAPDH served as the housekeeping gene to normalize expression of the tested genes. With the SYBR Green method primer, sequences for the genes were validated by dissociation curve/melt curve analysis. The $2^{-\Delta\Delta C_t}$ method was used for analysis of gene expression. Statistical analysis was carried out using the Tukey−Kramer multiple comparisons post-test analysis of variance (ANOVA). The relative transcript levels were expressed as the mean ± standard deviation ($n = 3$ for each group) for graph representation.

Microarray. Briefly, the cells were cultured in the Petri dishes (stimulated and control, three replicates of each) for 7 days. The cells were then lysed, and total RNA was extracted using a Qiagen RNeasy kit (Qiagen, UK). Gene expression changes were detected by hybridization of mRNA to Affymetrix HuGene 1.0 ST human arrays according to the manufacturer's instructions. Initial bioinformatic analysis was based on rank product,[72] and a false discovery rate of 20% was used to upload selected gene changes to the Ingenuity Pathway Analysis (IPA) server to identify (1) canonical signaling pathways, (2) functional pathways, and (3) to produce networks. IPA uses pathway libraries derived from the scientific literature. Statistics for functional analysis were carried out by Fischer's exact test (as done automatically by the software).

Conflict of Interest: The authors declare no competing financial interest.

Acknowledgment. We would like to thank the Ministry of Health and Medical Education of I.R. Iran for funding this project. We would like to thank Linn Products Ltd, Prof. Rein Ulijn, Prof. James Hough, Prof. James Faller, and Dr. Fiona Henriquez for useful discussions and their interest in this work. We are grateful for the additional financial support provided by BBSRC, STFC, the University of Glasgow, and the University of the West of Scotland. We also thank the Royal Society of Edinburgh and the Scottish Government for providing a research fellowship for S.R. We also thank Carol-Anne Smith, Peter Chung, and Margaret Mullin for laboratory assistance.

Supporting Information Available: Additional figures. This material is available free of charge *via* the Internet at http://pubs.acs.org.

REFERENCES AND NOTES

1. Dalby, M. J.; Yarwood, S. J.; Riehle, M. O.; Johnstone, H. J. H.; Affrossman, S.; Curtis, A. S. G. Increasing Fibroblast Response to Materials Using Nanotopography: Morphological and Genetic Measurements of Cell Response to 13-nm-High Polymer Demixed Islands. *Exp. Cell Res.* **2002**, *276*, 1–9.
2. Dalby, M. J.; Riehle, M. O.; Johnstone, H.; Affrossman, S.; Curtis, A. S. G. *In Vitro* Reaction of Endothelial Cells to Polymer Demixed Nanotopography. *Biomaterials* **2002**, *23*, 2945–2954.
3. Andersson, A. S.; Backhed, F.; von Euler, A.; Richter-Dahlfors, A.; Sutherland, D.; Kasemo, B. Nanoscale Features Influence Epithelial Cell Morphology and Cytokine Production. *Biomaterials* **2003**, *24*, 3427–3436.
4. Yim, E. K.; Reano, R. M.; Pang, S. W.; Yee, A. F.; Chen, C. S.; Leong, K. W. Nanopattern-Induced Changes in Morphology and Motility of Smooth Muscle Cells. *Biomaterials* **2005**, *26*, 5405–5413.
5. Child, H. W.; Del Pino, P. A.; De La Fuente, J. M.; Hursthouse, A. S.; Stirling, D.; Mullen, M.; McPhee, G. M.; Nixon, C.; Jayawarna, V.; Berry, C. C. Working Together: The Combined Application of a Magnetic Field and Penetratin for the Delivery of Magnetic Nanoparticles to Cells in 3D. *ACS Nano* **2011**, *5*, 7910–7919.
6. Conde, J.; Ambrosone, A.; Sanz, V.; Hernandez, Y.; Marchesano, V.; Tian, F.; Child, H.; Berry, C. C.; Ibarra, M. R.; Baptista, P. V.; *et al.* Design of Multifunctional Gold Nanoparticles for *In Vitro* and *In Vivo* Gene Silencing. *ACS Nano* **2012**, *6*, 8316–8324.
7. Yim, E. K.; Pang, S. W.; Leong, K. W. Synthetic Nanostructures Inducing Differentiation of Human Mesenchymal Stem Cells into Neuronal Lineage. *Exp. Cell Res.* **2007**, *313*, 1820–1829.
8. Yim, E. K.; Darling, E. M.; Kulangara, K.; Guilak, F.; Leong, K. W. Nanotopography-Induced Changes in Focal Adhesions, Cytoskeletal Organization, and Mechanical Properties of Human Mesenchymal Stem Cells. *Biomaterials* **2010**, *31*, 1299–1306.
9. Oh, S.; Brammer, K. S.; Li, Y. S.; Teng, D.; Engler, A. J.; Chien, S.; Jin, S. Stem Cell Fate Dictated Solely by Altered Nanotube Dimension. *Proc. Natl. Acad. Sci. U.S.A.* **2009**, *106*, 2130–2135.
10. Dalby, M. J.; Gadegaard, N.; Tare, R.; Andar, A.; Riehle, M. O.; Herzyk, P.; Wilkinson, C. D. W.; Oreffo, R. O. C. The Control of Human Mesenchymal Cell Differentiation Using Nanoscale Symmetry and Disorder. *Nat. Mater.* **2007**, *6*, 997–1003.
11. McMurray, R. J.; Gadegaard, N.; Tsimbouri, P. M.; Burgess, K. V.; McNamara, L. E.; Tare, R.; Murawski, K.; Kingham, E.; Oreffo, R. O.; Dalby, M. J. Nanoscale Surfaces for the Long-Term Maintenance of Mesenchymal Stem Cell Phenotype and Multipotency. *Nat. Mater.* **2011**, *10*, 637–644.
12. Tare, R. S.; Babister, J. C.; Kanczler, J.; Oreffo, R. O. Skeletal Stem Cells: Phenotype, Biology and Environmental Niches Informing Tissue Regeneration. *Mol. Cell. Endocrinol.* **2008**, *288*, 11–21.
13. Huang, G. T.; Gronthos, S.; Shi, S. Mesenchymal Stem Cells Derived from Dental Tissues *vs.* Those from Other Sources: Their Biology and Role in Regenerative Medicine. *J. Dent. Res.* **2009**, *88*, 792–806.
14. Schaffler, A.; Buchler, C. Concise Review: Adipose Tissue-Derived Stromal Cells—Basic and Clinical Implications for Novel Cell-Based Therapies. *Stem Cells* **2007**, *25*, 818–827.
15. Longo, U. G.; Loppini, M.; Berton, A.; La Verde, L.; Khan, W. S.; Denaro, V. Stem Cells from Umbilical Cord and Placenta for Musculoskeletal Tissue Engineering. *Curr. Stem Cell Res. Ther.* **2012**, *7*, 272–281.

16. Vater, C.; Kasten, P.; Stiehler, M. Culture Media for the Differentiation of Mesenchymal Stromal Cells. *Acta Biomater.* **2011**, *7*, 463–477.
17. Liu, J.; Song, L.; Jiang, C.; Liu, Y.; George, J.; Ye, H.; Cui, Z. Electrophysiological Properties and Synaptic Function of Mesenchymal Stem Cells During Neurogenic Differentiation: A Mini-Review. *Int. J. Artif. Organs* **2012**, *35*, 323–337.
18. Tsimbouri, P. M.; McMurray, R. J.; Burgess, K. V.; Alakpa, E. V.; Reynolds, P. M.; Murawski, K.; Kingham, E.; Oreffo, R. O.; Gadegaard, N.; Dalby, M. J. Using Nanotopography and Metabolomics To Identify Biochemical Effectors of Multipotency. *ACS Nano* **2012**, *6*, 10239–10249.
19. Biggs, M. J. P.; Richards, R. G.; Gadegaard, N.; Wilkinson, C. D. W.; Oreffo, R. O. C.; Dalby, M. J. The Use of Nanoscale Topography To Modulate the Dynamics of Adhesion Formation in Primary Osteoblasts and Erk/Mapk Signalling in Stro-1+Enriched Skeletal Stem Cells. *Biomaterials* **2009**, *30*, 5094–5103.
20. Engler, A. J.; Sen, S.; Sweeney, H. L.; Discher, D. E. Matrix Elasticity Directs Stem Cell Lineage Specification. *Cell* **2006**, *126*, 677–689.
21. McBeath, R.; Pirone, D. M.; Nelson, C. M.; Bhadriraju, K.; Chen, C. S. Cell Shape, Cytoskeletal Tension, and RhoA Regulate Stem Cell Lineage Commitment. *Dev. Cell* **2004**, *6*, 483–495.
22. Gao, L.; McBeath, R.; Chen, C. S. Stem Cell Shape Regulates a Chondrogenic *versus* Myogenic Fate through Rac1 and N-Cadherin. *Stem Cells* **2010**, *28*, 564–572.
23. Kilian, K. A.; Bugarija, B.; Lahn, B. T.; Mrksich, M. Geometric Cues for Directing the Differentiation of Mesenchymal Stem Cells. *Proc. Natl. Acad. Sci. U.S.A.* **2010**, *107*, 4872–4877.
24. Sawada, Y.; Sheetz, M. P. Force Transduction by Triton Cytoskeletons. *J. Cell Biol.* **2002**, *156*, 609–615.
25. Galbraith, C. G.; Yamada, K. M.; Sheetz, M. P. The Relationship between Force and Focal Complex Development. *J. Cell Biol.* **2002**, *159*, 695–705.
26. Vogel, V.; Sheetz, M. Local Force and Geometry Sensing Regulate Cell Functions. *Nat. Rev. Mol. Cell. Biol.* **2006**, *7*, 265–275.
27. Sawada, Y.; Tamada, M.; Dubin-Thaler, B. J.; Cherniavskaya, O.; Sakai, R.; Tanaka, S.; Sheetz, M. P. Force Sensing by Mechanical Extension of the Src Family Kinase Substrate P130cas. *Cell* **2006**, *127*, 1015–1026.
28. del Rio, A.; Perez-Jimenez, R.; Liu, R.; Roca-Cusachs, P.; Fernandez, J. M.; Sheetz, M. P. Stretching Single Talin Rod Molecules Activates Vinculin Binding. *Science* **2009**, *323*, 638–641.
29. Biggs, M. J. P.; Richards, R. G.; McFarlane, S.; Wilkinson, C. D. W.; Oreffo, R. O. C.; Dalby, M. J. Adhesion Formation of Primary Human Osteoblasts and the Functional Response of Mesenchymal Stem Cells to 330 nm Deep Microgrooves. *J. R. Soc. Interface* **2008**, *5*, 1231–1242.
30. Biggs, M. J. P.; Richards, R. G.; Gadegaard, N.; McMurray, R. J.; Affrossman, S.; Wilkinson, C. D. W.; Oreffo, R. O. C.; Dalby, M. J. Interactions with Nanoscale Topography: Adhesion Quantification and Signal Transduction in Cells of Osteogenic and Multipotent Lineage. *J. Biomed. Mater. Res., Part A* **2009**, *91A*, 195–208.
31. Pierres, A.; Benoliel, A. M.; Touchard, D.; Bongrand, P. How Cells Tiptoe on Adhesive Surfaces before Sticking. *Biophys. J.* **2008**, *94*, 4114–4122.
32. Guilak, F.; Cohen, D. M.; Estes, B. T.; Gimble, J. M.; Liedtke, W.; Chen, C. S. Control of Stem Cell Fate by Physical Interactions with the Extracellular Matrix. *Cell Stem Cell* **2009**, *5*, 17–26.
33. Park, S. H.; Sim, W. Y.; Min, B. H.; Yang, S. S.; Khademhosseini, A.; Kaplan, D. L. Chip-Based Comparison of the Osteogenesis of Human Bone Marrow- and Adipose Tissue-Derived Mesenchymal Stem Cells under Mechanical Stimulation. *PLoS ONE* **2012**, *7*, e46689.
34. Shi, Y.; Fu, Y.; Tong, W.; Geng, Y.; Lui, P. P.; Tang, T.; Zhang, X.; Dai, K. Uniaxial Mechanical Tension Promoted Osteogenic Differentiation of Rat Tendon-Derived Stem Cells (Rtdscs) *via* the Wnt5a-RhoA Pathway. *J. Cell. Biochem.* **2012**, *113*, 3133–3142.
35. Pingguan-Murphy, B.; Lee, D. A.; Bader, D. L.; Knight, M. M. Activation of Chondrocytes Calcium Signalling by Dynamic Compression Is Independent of Number of Cycles. *Arch. Biochem. Biophys.* **2005**, *444*, 45–51.
36. Knight, M. M.; van de Breevaart Bravenboer, J.; Lee, D. A.; van Osch, G. J.; Weinans, H.; Bader, D. L. Cell and Nucleus Deformation in Compressed Chondrocyte-Alginate Constructs: Temporal Changes and Calculation of Cell Modulus. *Biochim. Biophys. Acta* **2002**, *1570*, 1–8.
37. Cheema, U.; Chuo, C.-P.; Sarathchandra, P.; Nazhat, S. N.; Brown, R. A. Engineering Functional Collagen Scaffolds: Cyclical Loading Increases Material Strength and Fibril Aggregation. *Adv. Funct. Mater.* **2007**, *17*, 2426–2431.
38. Eastwood, M.; McGrouther, D. A.; Brown, R. A. Fibroblast Responses to Mechanical Forces. *Proc. Inst. Mech. Eng., Part H* **1998**, *212*, 85–92.
39. Kanaka, T. S.; Kumar, M. M. Neural Stimulation for Spinal Spasticity. *Paraplegia* **1990**, *28*, 399–405.
40. Chen, I. I.; Saha, S. Analysis of the Current Distribution in Bone Produced by Pulsed Electro-Magnetic Field Stimulation of Bone. *Biomater. Artif. Cells Artif. Organs* **1987**, *15*, 737–744.
41. Pompeiano, O.; Wand, P.; Sontag, K. H. The Sensitivity of Renshaw Cells to Velocity of Sinusoidal Stretches of the Triceps Surae Muscle. *Arch. Ital. Biol.* **1975**, *113*, 280–294.
42. Ingber, D. E. Tensegrity and Mechanotransduction. *J. Bodyw. Mov. Ther.* **2008**, *12*, 198–200.
43. Ward, D. F., Jr.; Salasznyk, R. M.; Klees, R. F.; Backiel, J.; Agius, P.; Bennett, K.; Boskey, A.; Plopper, G. E. Mechanical Strain Enhances Extracellular Matrix-Induced Gene Focusing and Promotes Osteogenic Differentiation of Human Mesenchymal Stem Cells through an Extracellular-Related Kinase-Dependent Pathway. *Stem Cells Dev.* **2007**, *16*, 467–480.
44. Hamilton, D. W.; Brunette, D. M. The Effect of Substratum Topography on Osteoblast Adhesion Mediated Signal Transduction and Phosphorylation. *Biomaterials* **2007**, *28*, 1806–1819.
45. Ge, C.; Xiao, G.; Jiang, D.; Franceschi, R. T. Critical Role of the Extracellular Signal-Regulated Kinase-Mapk Pathway in Osteoblast Differentiation and Skeletal Development. *J. Cell Biol.* **2007**, *176*, 709–718.
46. Xiao, G.; Jiang, D.; Gopalakrishnan, R.; Franceschi, R. T. Fibroblast Growth Factor 2 Induction of the Osteocalcin Gene Requires Mapk Activity and Phosphorylation of the Osteoblast Transcription Factor, Cbfa1/Runx2. *J. Biol. Chem.* **2002**, *277*, 36181–36187.
47. Willis, D. M.; Loewy, A. P.; Charlton-Kachigian, N.; Shao, J.-S.; Ornitz, D. M.; Towler, D. A. Regulation of Osteocalcin Gene Expression by a Novel Ku Antigen Transcription Factor Complex. *J. Biol. Chem.* **2002**, *277*, 37280–37291.
48. Stein, G. S.; Lian, J. B. Molecular Mechanisms Mediating Proliferation/Differentiation Interrelationships during Progressive Development of the Osteoblast Phenotype. *Endocr. Rev.* **1993**, *14*, 424–442.
49. Huang, Y. F.; Lin, J. J.; Lin, C. H.; Su, Y.; Hung, S. C. C-Jun N-Terminal Kinase 1 Negatively Regulates Osteoblastic Differentiation Induced by Bmp2 *via* Phosphorylation of Runx2 at Ser104. *J. Bone Miner. Res.* **2012**, *27*, 1093–1105.
50. Jang, W. G.; Kim, E. J.; Kim, D. K.; Ryoo, H. M.; Lee, K. B.; Kim, S. H.; Choi, H. S.; Koh, J. T. Bmp2 Protein Regulates Osteocalcin Expression *via* Runx2-Mediated Atf6 Gene Transcription. *J. Biol. Chem.* **2012**, *287*, 905–915.
51. Kim, W. K.; Meliton, V.; Bourquard, N.; Hahn, T. J.; Parhami, F. Hedgehog Signaling and Osteogenic Differentiation in Multipotent Bone Marrow Stromal Cells Are Inhibited by Oxidative Stress. *J. Cell. Biochem.* **2010**, *111*, 1199–1209.
52. Dai, Z.; Li, Y.; Quarles, L. D.; Song, T.; Pan, W.; Zhou, H.; Xiao, Z. Resveratrol Enhances Proliferation and Osteoblastic Differentiation in Human Mesenchymal Stem Cells *via* ER-Dependent ERK1/2 Activation. *Phytomedicine* **2007**, *14*, 806–814.
53. James, A. W.; Leucht, P.; Levi, B.; Carre, A. L.; Xu, Y.; Helms, J. A.; Longaker, M. T. Sonic Hedgehog Influences the

Balance of Osteogenesis and Adipogenesis in Mouse Adipose-Derived Stromal Cells. *Tissue Eng., Part A* **2010**, *16*, 2605–2616.
54. Day, T. F.; Yang, Y. Wnt and Hedgehog Signaling Pathways in Bone Development. *J. Bone Joint Surg. Am.* **2008**, *90 Suppl 1*, 19–24.
55. Pierres, A.; Monnet-Corti, V.; Benoliel, A. M.; Bongrand, P. Do Membrane Undulations Help Cells Probe the World? *Trends Cell. Biol.* **2009**, *19*, 428–433.
56. Evans, E. Kinetics of Granulocyte Phagocytosis: Rate Limited by Cytoplasmic Viscosity and Constrained by Cell Size. *Cell Motil. Cytoskeleton* **1989**, *14*, 544–551.
57. Shamri, R.; Grabovsky, V.; Gauguet, J. M.; Feigelson, S.; Manevich, E.; Kolanus, W.; Robinson, M. K.; Staunton, D. E.; von Andrian, U. H.; Alon, R. Lymphocyte Arrest Requires Instantaneous Induction of an Extended Lfa-1 Conformation Mediated by Endothelium-Bound Chemokines. *Nat. Immunol.* **2005**, *6*, 497–506.
58. Rappaz, B.; Barbul, A.; Hoffmann, A.; Boss, D.; Korenstein, R.; Depeursinge, C.; Magistretti, P. J.; Marquet, P. Spatial Analysis of Erythrocyte Membrane Fluctuations by Digital Holographic Microscopy. *Blood Cells, Mol., Dis.* **2009**, *42*, 228–232.
59. Evans, J.; Gratzer, W.; Mohandas, N.; Parker, K.; Sleep, J. Fluctuations of the Red Blood Cell Membrane: Relation to Mechanical Properties and Lack of ATP Dependence. *Biophys. J.* **2008**, *94*, 4134–4144.
60. Krol, A.; Grinfeldt, M. G.; Levin, S. V.; Smilgavichus, A. D. Local Mechanical Oscillations of the Cell Surface within the Range 0.2−30 Hz. *Eur. Biophys. J.* **1990**, *19*, 93–99.
61. Pelling, A. E.; Veraitch, F. S.; Pui-Kei Chu, C.; Nicholls, B. M.; Hemsley, A. L.; Mason, C.; Horton, M. A. Mapping Correlated Membrane Pulsations and Fluctuations in Human Cells. *J. Mol. Recognit.* **2007**, *20*, 467–475.
62. Szabo, B.; Selmeczi, D.; Kornyei, Z.; Madarasz, E.; Rozlosnik, N. Atomic Force Microscopy of Height Fluctuations of Fibroblast Cells. *Phys. Rev. E* **2002**, *65*, 041910.
63. Reinish, G. B.; Nowick, A. S. Piezoelectric Properties of Bone as Functions of Moisture Content. *Nature* **1975**, *253*, 626–627.
64. Finkelstein, E. I.; Chao, P. H.; Hung, C. T.; Bulinski, J. C. Electric Field-Induced Polarization of Charged Cell Surface Proteins Does Not Determine the Direction of Galvanotaxis. *Cell Motil. Cytoskeleton* **2007**, *64*, 833–846.
65. Mycielska, M. E.; Djamgoz, M. B. Cellular Mechanisms of Direct-Current Electric Field Effects: Galvanotaxis and Metastatic Disease. *J. Cell. Sci.* **2004**, *117*, 1631–1639.
66. Goldstein, C.; Sprague, S.; Petrisor, B. A. Electrical Stimulation for Fracture Healing: Current Evidence. *J. Orthop. Trauma* **2010**, *24 Suppl 1*, S62–S65.
67. Noris-Suarez, K.; Lira-Olivares, J.; Ferreira, A. M.; Feijoo, J. L.; Suarez, N.; Hernandez, M. C.; Barrios, E. *In Vitro* Deposition of Hydroxyapatite on Cortical Bone Collagen Stimulated by Deformation-Induced Piezoelectricity. *Biomacromolecules* **2007**, *8*, 941–948.
68. Fernandez, J. R.; Garcia-Aznar, J. M.; Martinez, R. Piezoelectricity Could Predict Sites of Formation/Resorption in Bone Remodelling and Modelling. *J. Theor. Biol.* **2012**, *292*, 86–92.
69. Wysocki, A.; Butler, M.; Shamliyan, T.; Kane, R. L. Whole-Body Vibration Therapy for Osteoporosis: State of the Science. *Ann. Intern. Med.* **2011**, *155*, 680–686W206-613.
70. Alizadeh-Meghrazi, M.; Masani, K.; Popovic, M. R.; Craven, B. C. Whole-Body Vibration During Passive Standing in Individuals with Spinal Cord Injury: Effects of Plate Choice, Frequency, Amplitude, and Subject's Posture on Vibration Propagation. *PM&R* **2012**, *4*, 963–975.
71. Tamma, R.; dell'Endice, S.; Notarnicola, A.; Moretti, L.; Patella, S.; Patella, V.; Zallone, A.; Moretti, B. Extracorporeal Shock Waves Stimulate Osteoblast Activities. *Ultrasound Med. Biol.* **2009**, *35*, 2093–2100.
72. Breitling, R.; Armengaud, P.; Amtmann, A.; Herzyk, P. Rank Products: A Simple, Yet Powerful, New Method To Detect Differentially Regulated Genes in Replicated Microarray Experiments. *FEBS Lett.* **2004**, *573*, 83–92.